Spintronic Memory and Logic

Design of Stochastic Nanomagnets for Probabilistic Spin Logic

Punyashloka Debashis[1,2], Rafatul Faria[1], Kerem Y. Camsari[1], and Zhihong Chen[1,2]

[1] School of Electrical and Computer Engineering, Purdue University, West Lafayette, IN 47907, USA
[2] Birck Nanotechnology Center, Purdue University, West Lafayette, IN 47907, USA

Received 30 May 2018, revised 27 Jun 2018, accepted 9 Jul 2018, published 27 Jul 2018, current version 27 Aug 2018.

Abstract—Probabilistic spin logic (PSL) is a new paradigm of computing that relies on probabilistic bits (p-bits) that fluctuate randomly between metastable states. PSL may be more efficient than conventional CMOS-based logic in terms of intrinsic optimization, Bayesian inference, invertible Boolean logic, and hardware machine learning. Effectively tunable random number generators, p-bits, can be realized as stochastic nanomagnets that can be made to prefer one state over others by an external input, such as voltage or current. This letter looks at the design of stochastic nanomagnets that is most suitable as p-bits for PSL. Experimental evidence, supported by theory and numerical simulation, shows that the scaling of magnetic anisotropy is more effective than the scaling of the net magnetic moment for voltage-driven PSL applications. A novel system that can be used as a tunable random number generator is demonstrated experimentally and analyzed theoretically: a magnet with perpendicular magnetic anisotropy that is initialized to its hard axis by giant spin Hall effect torque. With zero external input, this system provides a potentially better alternative to other nanomagnet-based random number generators. By tuning the randomness through an external input, this system is suitable for probabilistic networks for Bayesian inference.

Index Terms—Spintronic memory and logic, nanomagnetics, probabilistic spin logic, low-barrier nanomagnet, hard-axis initialization.

I. INTRODUCTION

Probabilistic spin logic (**PSL**) is a new computing paradigm that has been theoretically shown to be more suitable than conventional CMOS for performing tasks such as intrinsic optimization, probabilistic inference from Bayesian networks, and invertible Boolean logic [Behin-Aein 2016, Camsari 2017, Debashis 2017, Faria 2017, Sutton 2017, Zand 2017]. PSL relies on unstable stochastic bits called probabilistic bits (**p-bits**) that are essentially random signal generators with a tunable mean output. They can either be analog (generating any random values between "0" and "1") or binary random number generators (generating randomly "0" or "1"). A stochastic nanomagnet with low barrier energy E_B can form a natural hardware for implementing the p-bit as its magnetization randomly fluctuates between its metastable states with an average retention time of [Lopez-Diaz 2002]

$$\tau = \tau_0 \exp\left(\frac{E_B}{k_B T}\right) \tag{1}$$

where τ_0 is the material-dependent parameter called the attempt time of the nanomagnet. The most commonly stated value for τ_0 in the literature is generally assumed to be between 10^{-11} s to 10^{-9} s [Lopez-Diaz 2002]. Hence, a low-barrier nanomagnet-based p-bit with $E_B \approx k_B T$ can produce random numbers at gigahertz speed. The mean value of magnetization (and as a result, the mean of the produced random numbers) can be tuned by an external input, such as spin current from the giant spin Hall effect (**GSHE**) [Camsari 2017, Faria 2017, Sutton 2017], spin transfer torque (**STT**) [Locatelli 2014, Vodenicarevic 2017], or an effective magnetic field from the magnetoelectric effect [Hassan 2018]. The ease of tunability is judged by evaluating the input required to pin the fluctuating magnetization state to one value. For example, the magnitude of the effective magnetic field generated by the electric field in the case of voltage control of magnetization [Manipatruni 2018] is an important metric for energy efficiency to achieve low-power computation. Significantly, both speed and energy consumption of the p-bit can be carefully engineered through proper design of the nanomagnet involved in the device.

In this letter, the following three methods to obtain stochastic nanomagnets have been explored: (1) by reduction of anisotropy; (2) by reduction of net magnetic moment; and (3) by hard-axis initialization.

In conjunction with Boltzmann theory and stochastic Landau–Lifshitz–Gilbert (**sLLG**) simulations, the first two methods are compared in terms of pinning field and speed. Finally, a novel method to generate random numbers with a tunable input, achieved by the hard-axis initialization of a perpendicular magnetic anisotropy (**PMA**) magnet, is demonstrated for the first time. Supported by the Fokker–Planck theory and sLLG simulations, its pinning field and speed are discussed.

II. STOCHASTICITY BY SCALING MOMENT AND SCALING ANISOTROPY

In order to make a fast stochastic nanomagnet that randomly fluctuates with an average retention time of 1 ns, its energy barrier E_B needs to be scaled to $\sim 1\ k_B T$, according to (1). Since E_B is a product of the anisotropy field H_K and the net moment $M_S \times$ Vol., both can be reduced to achieve an energy barrier of $1\ k_B T$. The response of such stochastic nanomagnets

Corresponding author: Punyashloka Debashis (e-mail: punya379@gmail.com).
Digital Object Identifier 10.1109/LMAG.2018.2860547

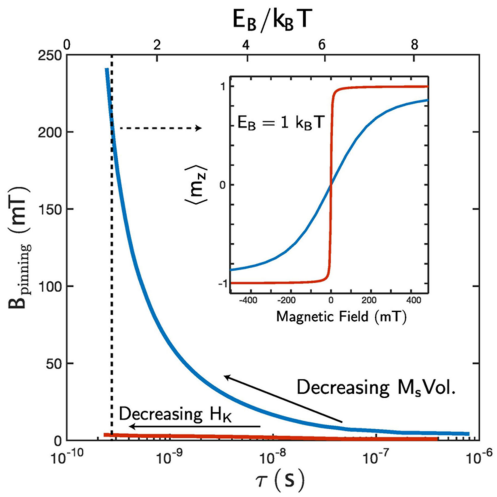

Fig. 1. Field required to pin a stochastic magnet versus the speed of fluctuation. Calculations based on Boltzmann law show that making magnets faster by scaling anisotropy (red curve) is more efficient than scaling net moment (blue curve) in terms of the field required to pin the scaled magnet. The inset shows the average magnetization versus *B*-field for a $1\ k_BT$ magnet. It suggests that the pinning field is much smaller for the case of magnet B (red curve) compared to magnet C (blue curve).

to magnetic fields can be captured by the following analysis based on the Boltzmann law.

The energy of a magnet in the macrospin limit under the application of an external *B*-field, H_{ext}, can be written as

$$E = 2\pi M_s^2\,(\text{Vol.})\,m_x^2 - H_{\text{ext}} M_s\,(\text{Vol.})\,m_z - \frac{1}{2} H_k M_s\,(\text{Vol.})\,m_z^2 \tag{2}$$

where $m_x = \sin(\theta)\cos(\phi)$ is the magnetization along the out-of-plane hard axis (x), $m_z = \cos(\theta)$ is that along the easy axis (z), θ being the angle of the magnetization direction with respect to the easy axis, M_s is the saturation magnetization, H_k is the uniaxial anisotropy along the z-axis, and Vol. is the volume of the magnet. The first, second, and third terms are contributions from the shape anisotropy, external magnetic field, and uniaxial anisotropy field, respectively.

The probability of finding the magnetization in (θ, ϕ) configuration can be found by the equilibrium Boltzmann distribution

$$p\ (\theta, \phi) = \frac{1}{Z} \exp\left(-\frac{E}{k_B T}\right) \tag{3}$$

where Z is a normalization constant.

The average magnetization along the z-axis can be written as

$$\langle m_z \rangle = \frac{\int_{\theta=0}^{\theta=\pi} \int_{\phi=-\pi}^{\phi=\pi} d\phi\ d\theta\ p\,(\theta, \phi)\ \cos(\theta)\ \sin(\theta)}{\int_{\theta=0}^{\theta=\pi} \int_{\phi=-\pi}^{\phi=\pi} d\phi\ d\theta\ p\,(\theta, \phi)\ \sin(\theta)}. \tag{4}$$

Based on the above-mentioned equations, Fig. 1 shows the plot of the field that is required to pin a stochastic nanomagnet as we scale its energy barrier. Scaling the H_K results in almost negligible change in pining field. However, scaling moments to smaller values results in much larger corresponding pinning fields.

The inset of Fig. 1 considers two magnets with $E_B = 1\ k_BT$ obtained by reducing H_K (red curve) and $M_S \times$ Vol. (blue curve), respectively. Compared to a stable 40 k_BT magnet, the first magnet has 40 times smaller H_K and the second has 40 times smaller moment. Even though both magnets have the same E_B, leading to the same time scale of fluctuation (τ), the field required to pin the low H_K is appreciably smaller than that for the low $M_S \times$ Vol. magnet (see inset of Fig. 1). Since this translates to a smaller energy requirement in a voltage-driven PSL [Hassan 2018] circuit, designing stochastic nanomagnets by reducing anisotropy seems to be the better option compared to reducing the volume. We then go on to test this theoretical prediction experimentally.

To compare the effect of reduced anisotropy versus reduced volume, it would be ideal to fabricate the two $1\ k_BT$ magnets, as described previously. However, in practice, it is challenging to make two stochastic nanomagnets that are 40 times different in net moment. Therefore, two nanomagnets that are about 4 times different in their net moment are fabricated in the following experiments.

A. Achieving Stochasticity by Reducing Anisotropy

Experimentally, a low H_K magnet is realized by a circular disk magnet of $Co_{60}Fe_{20}B_{20}$ with a diameter of 110 nm and thickness of 1.3 nm. Circular disk in-plane magnets have been proposed as p-bits [Debashis 2017, Faria 2017], as they fluctuate in random in-plane directions as a function of time. Such a stochastic element has been realized in our experiments with monodomain circular disk nanomagnets [Cowburn 1999, Debashis 2017] with careful material and design choices, guided by the tradeoff between exchange stiffness and dipolar self-energy [Brown 1968]. Starting from a sputter deposited stack of Ta(15)/CoFeB(1.5)/MgO(1)/Ru(4) (thicknesses in nanometers), an array of 25 million nominally identical circular disk nanomagnets is fabricated using e-beam lithography and Ar ion milling. Then, their response is measured using a superconducting quantum interference device in Quantum Design MPMS-3. Fig. 2(a) shows the scanning electron microscopy (**SEM**) image of a portion of the array. Fig. 2(b) shows a hysteresis-free, sigmoidal output curve of the average magnetization of the array. It should be noted here that although the average steady-state behavior is determined completely by the applied magnetic field, the time-domain behavior of each nanomagnet is stochastic, owing to their low energy barrier. Such individually stochastic units whose average behavior exhibits a sigmoidal response as a function of an input parameter can be used as a building block for a class of stochastic neural networks in machine learning [Ackley 1987] among other PSL applications.

B. Achieving Stochasticity by Reducing Moment

Next, an array of 100 million elliptical nanomagnets is fabricated using e-beam lithography, physical evaporation of Permalloy (**Py**), followed by liftoff. Since they are elliptical, shape anisotropy [Cowburn 2000] creates a large H_K. Hence, to reach stochasticity, the net moment has to be reduced to obtain small E_B. This is achieved in our magnets with dimensions of 49 nm $\times$ 61 nm $\times$ 5 nm. Also, through heat treatment (heating to 400 K for 1 h, then at 500 K for another hour, followed by cool down to room temperature, all at $\sim$150 mTorr pressure in Helium), reduced saturation magnetization of 250 kA/m is obtained for our Py nanomagnets. Fig. 2(c) shows the SEM

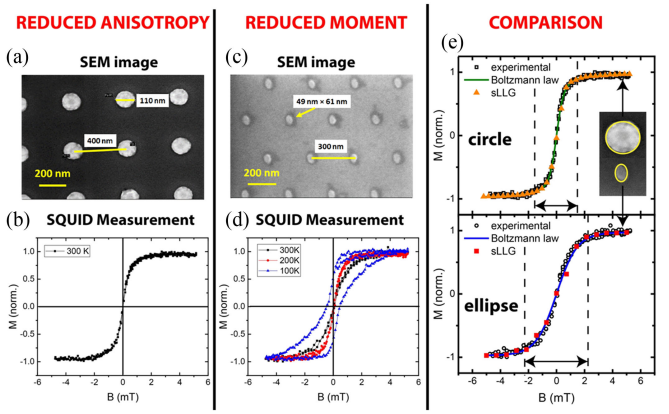

Fig. 2. Two methods of reducing energy barrier: anisotropy reduction and net magnetic moment reduction. (a) SEM of the array of CoFeB circular disk magnets. (b) Normalized magnetization response to applied magnetic field. The sigmoid shape with no remanence at zero field and saturation behavior is reminiscent of tunable stochastic behavior. (c) SEM of the array of Py elliptical magnets. (d) Normalized magnetization response to applied magnetic field for various temperatures. The sigmoid gets sharper for a lower temperature and eventually a hysteresis behavior is observed as the magnet fluctuations slow down. (e) Comparison of the two magnet behaviors matched with predictions by LLG simulations and Boltzmann law with experimental parameters. The required pinning field for the circular disk magnet is 20% less compared to that for the elliptical magnet, despite the fact that the former magnet has 4 times more $M_S \times$ Vol. compared to the latter magnet.

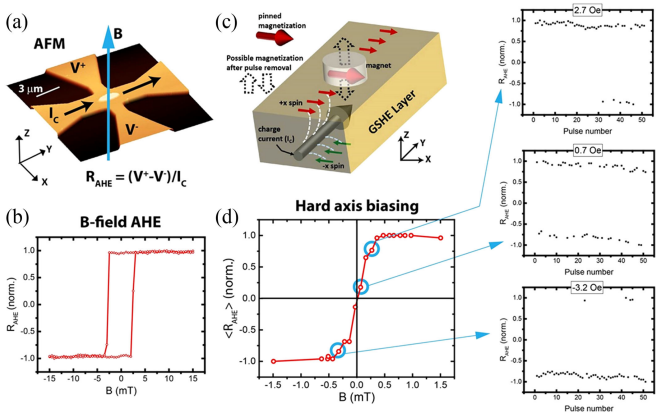

Fig. 3. Tunable random number generator from hard-axis initialization of a PMA magnet. (a) AFM of the fabricated device with marked current, voltage, and external magnetic field directions. The AHE resistance is calculated by taking the ratio of the voltage developed and the charge current supplied. (b) R_{AHE} as a function of external B field. The hysteretic behavior is indicative of a good, stable PMA magnetic behavior. (c) Cartoon depicting the physical picture of hard-axis initialization. (d) Sigmoid obtained by putting the PMA magnet in hard axis by GHSE torque and then letting it relax back to either "up" or "down" position in the presence of a small external field along the z-axis. Each point in this curve is obtained by taking the average of 51 GSHE pulsing events. Three indicative points are shown in the three panels to the right-hand side of the graph.

picture of an array of such nanomagnets. At 300 K, E_B is small enough to make the magnets stochastic, resulting in a sigmoid-curve-shaped normalized magnetization shown in Fig. 2(d) with black curve. Using experimentally measured saturation magnetization and magnet volume, H_K of 25 mT can be extracted by fitting the curve with a sigmoid function obtained from the Boltzmann law. This then results in $E_B \approx 9\ k_B T$ and consequently $\tau \approx 8$ μs (assuming $\tau_0 = 1$ ns). Since our conclusion from this experiment relies on the fact that these elliptical magnets have large anisotropy, H_K obtained from fitting needs justification. To ensure that the fitted value of H_K is reasonable, further measurements at reduced temperatures are carried out. A sigmoidal response is still observed at $T = 200$ K with a sharper slope (see Fig. 2(d), red curve), consistent with the expectation from the Boltzmann law. Finally, at $T = 100$ K, magnets are essentially frozen and the ensemble behaves like a ferromagnet, showing hysteretic magnetization response to the applied field with a clear remanence at $B = 0$ T (see Fig. 2(d), blue curve). Considering the saturation magnetization, magnet volume, and the fact that the magnetization of these nanomagnets transition from being stochastic to stable in a temperature window between 100 and 200 K, the bounds for H_K are estimated to be between 10 and 30 mT, which is consistent with the fitted H_K value of 25 mT. Both sigmoidal curves at 300 and 200 K show excellent agreement with the Boltzmann law using the same set of H_K and M_S with temperature corrections.

C. Comparing the Two Methods

Using the experimentally measured values of M_S and Vol., the net moment $M_S \times \mathrm{Vol.} = 1.2 \times 10^{-17}$ A·m^2 and 0.3×10^{-17} A·m^2 are calculated for the CoFeB circular disk magnet and the Py elliptical magnet, respectively. As expected, when the two scaling methods are compared in Fig. 2(e), the pinning field for the circular disk magnet is 20% smaller than that of the elliptical one, despite its $M_S \times$ Vol. being 4 times larger. This is also confirmed by stochastic LLG simulations. The excellent agreement between experiment, Boltzmann law, and stochastic LLG simulations for both circular disk and elliptical magnets is shown in Fig. 2(e).

Since the circular disk magnet has negligible E_B because of the absence of a shape anisotropy, as long as the circular disk magnet is small enough to behave as a monodomain body by avoiding vortex formation, its fluctuation time scale is limited by τ_0, unlike the elliptical magnet [see (1)]. Hence, the circular disk magnet is both faster and consumes lower energy by requiring a smaller pinning field, compared to the elliptical magnet.

III. STOCHASTICITY BY HARD-AXIS INITIALIZATION OF A PERPENDICULAR ANISOTRPY MAGNET

Now, a thermally stable PMA magnet whose easy axis is along the z-axis is considered. It is initialized along its hard-axis direction (xy plane) by means of an external force. When the external force is removed, the magnet makes a stochastic choice to fall into one of the two stable states along its easy axis. When this is done in the presence of a small external z-directed magnetic field, the magnetization prefers one state over the other, producing the sigmoidal curve for the average magnetization.

To test this idea, tantalum Hall bar devices with a PMA magnet island at the center are fabricated from a stack of Ta(10)/CoFeB(1)/MgO(1.5)/Ta(5) (thicknesses in nanometers) by successive lithography and ion milling steps, as shown in the AFM image of Fig. 3 (a). A charge current in the "y"-

direction produces a voltage along the "x"-direction due to the anomalous Hall effect (**AHE**) of the PMA magnet, where the sign of this voltage depends on whether the magnet is pointing "up" ($+z$-direction) or "down" ($-z$-direction). We use this method to read the magnetization direction of the PMA magnet. Fig. 3(b) shows the measured hysteresis loop of the PMA magnet by means of AHE with an external field sweeping in the "z"-direction.

Next, an efficient way to put a PMA magnet in its hard axis and releasing it is demonstrated in the following experiment. It is well understood that a moderate current pulse along the y-axis of Ta can produce a spin transfer torque to the PMA magnet along the x-axis and cause its magnetization rotation in the yz plane [Liu 2012a]. However, when a large current pulse ($J = 3.1 \times 10^7 \text{A/ cm}^2$) is applied through the Hall bar, the spin torque becomes so large that the PMA magnet can develop a magnetization along the x-direction, as predicted by Liu [2012b]. Once the large torque is released, the PMA magnet will go back to one of its easy axis magnetizations by random choices [see Fig. 3(c)], which can be monitored by the R_{AHE} reading. This pulsing is repeated several times to show the complete randomness of the two R_{AHE} states after each pulse. A similar experiment was performed by Bhowmik [2014] for spin Hall clocking of nanomagnetic logic. Furthermore, a small out-of-plane magnetic field is applied and the above-mentioned, procedure is repeated. The plot of the average magnetization after 51 pulsing events for each applied magnetic field is shown in Fig. 3(d). Here, the average magnetization is calculated by

$$\langle R_{\text{AHE}} \rangle = \frac{1}{N} \Sigma \left(\frac{R_{\text{AHE}}}{|R_{\text{AHE}}|} \right) \tag{5}$$

where N is the number of pulsing events (51 in this case). The subplots of Fig. 3(d) show the individual pulsing events for each point on the sigmoidal curve. This shows that at any given magnetic field B, the magnetization of the PMA magnet after releasing from its hard axis behaves stochastically, with an overall mean that is tunable by the magnetic field.

Next, the observed experimental hard-axis initialization of PMA magnets is systematically analyzed using stochastic LLG simulations. In the absence of any magnetic fields the critical current to place a PMA magnet in its hard axis is of the order of $I_{\text{SC}} = \frac{2q}{\hbar} M_S \text{Vol.} \frac{H_K}{2}$ [Fukami 2016]. We apply repeated current pulses of this magnitude to obtain the average magnetization in the presence of thermal noise and a z-directed external magnetic field that is on the entire time (see Fig. 4 inset). Three different spin-current pulses are investigated based on how fast they are turned off. In the case of the fast turn off, the magnetization dynamics can be directly solved by a one-dimensional Fokker–Planck equation (**FPE**) [Butler 2012] that describes the exact evolution of the ensemble, since when the spin current is off, the external magnetic field and the anisotropy are both in the $\pm z$ direction. The FPE equation for a z-directed PMA magnet is described by

$$\frac{\partial p(m_z, \tau_N)}{\partial \tau_N} = \frac{\partial}{\partial m_z} \left[(i - h - m_z)\left(1 - m_z^2\right) p + \frac{1 - m_z^2}{2E_B} \frac{\partial p}{\partial m_z} \right].$$

Here, i is the normalized z-polarized spin current I_s/I_{sc} where $I_{\text{sc}} = 4q/\hbar \ \alpha E_B(kT)$ with α being the damping

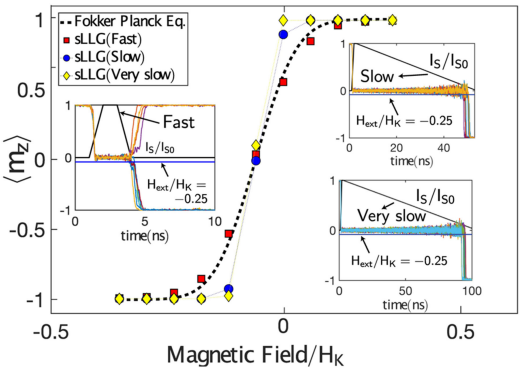

Fig. 4. Stochastic LLG simulations of a hard-axis initialized PMA magnet. At each point, at least $N = 200$ samples are recorded, and an average magnetization is obtained as in the experiment.

coefficient and E_B being the thermal energy barrier of the magnet; h is the normalized z-directed external magnetic field H_{ext}/H_k; τ_N is a normalized time which is related to the real time t by $t = \tau_N (1 + \alpha^2)/\alpha\gamma H_k$. After the x-polarized GSHE spin current is turned off, $i = 0$ in the FPE equation.

The FPE is solved starting from the time when the pulse is turned off, with an initial condition $p(m_z, \ \tau_N = 0)$ that places the initial probability distribution to the hard axis, approximated by a Gaussian distribution of $p(m_z)$ with mean zero and a very small standard deviation. For a fast turn off of the spin current, FPE is in good agreement with a direct stochastic LLG simulation. This suggests that the slope of the sigmoid depends only on the energy barrier (E_B) and the ratio of the external magnetic field to the anisotropy field (H/H_K), since these are the only parameters that enter the FPE. So, for a given energy barrier, having a lower H_K results in a smaller pinning field, as evident from the x-axis of Fig. 4.

The speed at which random numbers can be generated by the hard axis initialization method is ultimately limited by the time it takes for the magnetization to relax back to one of the stable states once released from the hard axis. This is determined by the natural time scale (τ_N) of the magnet mentioned earlier, and is independent of its energy barrier, unlike the case of low-barrier magnets. Second, since the randomization occurs when the magnet relaxes from its hard axis and is not affected by any prior events, the pulse rise time t_{rise} and the pulsewidth t_{ON} does not affect the process if their sum is larger than τ_N. However, the pulse fall time (t_{fall}) affects the process of magnetization relaxation from the hard axis. We observed that for slow current the ramp down the sigmoidal curve becomes sharper. The inset of Fig. 4 illustrates this behavior for ten samples for different spin-current pulses at a slightly negative magnetic field.

Second, this method provides a potentially better alternate to the STT-MTJ-based true random number generators (**TRNGs**) [Fukushima 2014]. In our case, the current pulse passes through the adjacent heavy metal layer (Ta) instead of passing through the tunnel barrier as in the case of STT-MTJ-based TRNGs, and hence, our device has potentially better endurance and capability of producing more random numbers. Also, compared to TRNGs based on superparamagnetic MTJs [Vodenicarevic 2017], this device does not require an external magnetic field to cancel the dipolar field from the reference layer.

ACKNOWLEDGMENT

The authors thank Prof. S. Datta and Prof. J. Appenzeller for many helpful discussions. This work was supported in part by the Center for Probabilistic Spin Logic for Low-Energy Boolean and Non-Boolean Computing, in part by one of the Nanoelectronic Computing Research Centers as task 2759.003 and 2759.004, and in part by a Semiconductor Research Corporation program sponsored by the National Science Foundation through CCF 1739635.

REFERENCES

Ackley D H, Hinton G E, Sejnowski T J (1987), "A learning algorithm for Boltzmann machines," in *Readings in Computer Vision*. Amsterdam, The Netherlands: Elsevier, pp. 522–533, doi: 10.1016/B978-0-08-051581-6.50053-2.

Behin-Aein B, Diep V, Datta S (2016), "A building block for hardware belief networks," *Sci. Rep.*, vol. 6, 29893, doi: 10.1038/srep29893.

Bhowmik D, You L, Salahuddin S (2014), "Spin Hall effect clocking of nanomagnetic logic without magnetic field," *Nature Nanotechnol.*, vol. 9, pp. 59–63, doi: 10.1038/nnano.2013.241.

Brown W F (1968), "The fundamental theorem of fine-ferromagnetic-particle theory," *J. Appl. Phys.*, vol. 39, pp. 993–994, doi: 10.1063/1.1656363.

Butler W H, Mewes T, Mewes C K A, Visscher P B, Rippard W H, Russek S E, Heindl R (2012), "Switching distributions for perpendicular spin-torque devices within the macrospin approximation," *IEEE Trans. Magn.*, vol. 48, pp. 4684–4700, doi: 10.1109/TMAG.2012.2209122.

Camsari K Y, Faria R, Sutton B M, Datta S (2017), "Stochastic p-bits for invertible logic," *Phys. Rev. X*, vol. 7, 031014, doi: 10.1103/PhysRevX.7.031014.

Cowburn R P (2000), "Property variation with shape in magnetic nanoelements," *J. Phys. D: Appl. Phys.*, vol. 33, pp. R1–R16, doi: 10.1088/0022-3727/33/1/201.

Cowburn R P, Koltsov D K, Adeyeye A O, Welland M E, Tricker D M (1999), "Single-domain circular nanomagnets," *Phys. Rev. Lett.*, vol. 83, pp. 1042–1045, doi: 10.1103/PhysRevLett.83.1042.

Debashis P, Faria R, Camsari K Y, Appenzeller J, Datta S, Chen Z (2017), "Experimental demonstration of nanomagnet networks as hardware for Ising computing," in *Proc. IEEE Int. Electron Devices Meeting*, pp. 34.3.1–34.3.4, doi: 10.1109/IEDM.2016.7838539

Faria R, Camsari K Y, Datta S (2017), "Low-barrier nanomagnets as p-bits for spin logic," *IEEE Magn. Lett.*, vol. 8, 4105305, doi: 10.1109/LMAG.2017.2685358.

Fukami S, Anekawa T, Zhang C, Ohno H (2016), "A spin-orbit torque switching scheme with collinear magnetic easy axis and current configuration," *Nature Nanotechnol.*, vol. 11, pp. 621–625, doi: 10.1038/nnano.2016.29.

Fukushima A, Seki T, Yakushiji K, Kubota H, Imamura H, Yuasa S, Ando K (2014), "Spin dice: A scalable truly random number generator based on spintronics," *Appl. Phys. Express*, vol. 7, 083001, doi: 10.7567/APEX.7.083001.

Hassan O, Camsari K Y, Datta S (2018), "Voltage-driven building block for hardware belief networks," unpublished paper. [Online]. Available: https://arxiv.org/abs/1801.09026v1.

Liu L, Pai C-F, Li Y, Tseng H W, Ralph D C, Buhrman R A (2012a), "Spin-torque switching with the giant spin Hall effect of tantalum," *Science*, vol. 336, pp. 555–558, doi: 10.1126/science.1218197.

Liu L, Lee O J, Gudmundsen T J, Ralph D C, Buhrman R A (2012b), "Current-induced switching of perpendicularly magnetized magnetic layers using spin torque from the spin Hall effect," *Phys. Rev. Lett.*, vol. 109, 096602, doi: 10.1103/PhysRevLett.109.096602.

Locatelli N, Mizrahi A, Accioly A, Matsumoto R, Fukushima A, Kubota H, Yuasa S, Cros V, Pereira L G, Querlioz D, Kim J-V, Grollier J (2014), "Noise-enhanced synchronization of stochastic magnetic oscillators," *Phys. Rev. Appl.*, vol. 2, 034009, doi: 10.1103/PhysRevApplied.2.034009.

Lopez-Diaz L, Torres L, Moro E (2002), "Transition from ferromagnetism to superparamagnetism on the nanosecond time scale," *Phys. Rev. B: Condens. Matter Mater. Phys.*, vol. 65, 224406, doi: 10.1103/PhysRevB.65.224406.

Manipatruni S, Nikonov D E, Lin C-C, Bhagwati P, Huang Y L, Damodaran A P, Chen Z, Ramesh R, Young I A (2018), "Voltage control of uni-directional anisotropy in ferromagnet-multiferroic system," unpublished paper. [Online]. Available: https://arxiv.org/abs/1801.08280v1.

Sutton B, Camsari K Y, Behin-Aein B, Datta S (2017), "Intrinsic optimization using stochastic nanomagnets," *Sci. Rep.*, vol. 7, 44370, doi: 10.1038/srep44370.

Vodenicarevic D, Locatelli N, Mizrahi A, Friedman J S, Vincent A F, Romera M, Fukushima A, Yakushiji K, Kubota H, Yuasa S, Tiwari S, Grollier J, Querlioz D (2017), "Low-energy truly random number generation with superparamagnetic tunnel junctions for unconventional computing," *Phys. Rev. Appl.*, vol. 8, 054045, doi: 10.1103/PhysRevApplied.8.054045.

Zand R, Camsari K Y, Ahmed I, Pyle S D, Kim C H, Datta S, DeMara R F (2017), "R-DBN: A resistive deep belief network architecture leveraging the intrinsic behavior of probabilistic devices," unpublished paper. [Online]. Available: https://arxiv.org/abs/1710.00249.